Clues to the Formation of Spiral Structure in M51 from the Ages and Locations of Star Clusters

Rupali Chandar[1], L.-H. Chien[2], Sharon Meidt[3], Miguel Querejeta[3], Clare Dobbs[4], Eva Schinnerer[3], Bradley C. Whitmore[5], Daniela Calzetti[6], Daiana Dinino[7], Robert C. Kennicutt[8], and Michael Regan[5]

[1] Department of Physics & Astronomy, The University of Toledo, Toledo, OH 43606, USA; Rupali.Chandar@utoledo.edu
[2] Northern Arizona University, Flagstaff, AZ 86001, USA
[3] Max-Planck-Institut für Astronomie, Königstuhl 17, D-69117 Heidelberg, Germany
[4] School of Physics, University of Exeter, Exeter EX4 4QL, UK
[5] Space Telescope Science Institute, Baltimore, MD 21218, USA
[6] Dept. of Astronomy, University of Massachusetts, Amherst, MA 01003, USA
[7] CICLOPS, Space Science Institute, 4750 Walnut Street, Boulder, CO 80301, USA
[8] Institute of Astronomy, Cambridge University, Cambridge, UK

Abstract

We determine the spatial distributions of star clusters at different ages in the grand-design spiral galaxy M51 using a new catalog based on multi-band images taken with the *Hubble Space Telescope* (*HST*). These distributions, when compared with the spiral structure defined by molecular gas, dust, young and old stars, show the following sequence in the inner arms: dense molecular gas (and dust) defines the inner edge of the spiral structure, followed by an overdensity of old stars and then young stellar clusters. The offset between gas and young clusters in the inner arms is consistent with the expectations for a density wave. Clusters as old as a few hundred Myr remain concentrated close to the spiral arms, although the distributions are broader than those for the youngest clusters, which is also consistent with predictions from density wave simulations. The outermost portion of the west arm is different from the rest of the spiral structure in that it contains primarily intermediate-age ($\approx$100–400 Myr) clusters; we believe that this is a "material" arm. We have identified four "feathers," stellar structures beyond the inner arms that have a larger pitch angle than the arms. We do not find age gradients along any of the feathers, but the least coherent feathers appear to have the largest range of cluster ages.

Key words: galaxies: individual (M51) – galaxies: star clusters: general – galaxies: starburst – stars: formation

1. Introduction

Dynamical structures within galaxies impact local star formation (e.g., Renaud et al. 2013; Emsellem et al. 2015). Grand-design spiral galaxies like M51 are an ideal place to study the interplay between gas density and motions, and how these impact the formation of stars and stellar clusters. Recent results suggest that dynamical structures like spiral arms and bars create deviations from axisymmetry in the gravitational potential that induce streaming motions, shear, and shocks in the gas (Meidt et al. 2013; Colombo et al. 2014a), which lead to changes in the local gas surface density and affect the organization and structure of the ISM down to the scales of giant molecular clouds (Hughes et al. 2013; Colombo et al. 2014b).

Stellar clusters, which form in regions of high gas density within galaxies, are one of the key products of star formation. Because they can be age-dated, their spatial distributions in a spiral galaxy like M51 provide direct information on the nature and timing of the molecular gas flow relative to the spiral arms. The locations of age-dated clusters relative to spiral structure traced by gas and old stars can also help to discriminate between different theoretical models for the formation of the arms, or at the very least show how the gravitational potential affects the movement of the clusters. For example, Roberts (1969) first explained that a quasi-stationary density wave should lead to a temporal sequence of events as material streams in and out of the spiral pattern. One observational signature of this sequence would be spatial offsets for star-forming tracers of different ages. To date, some works have

found evidence for such spatial offsets (e.g., Tamburro et al. 2008; Egusa et al. 2009), while others have not (e.g., Foyle et al. 2011).

The PAWS survey has provided an unprecedented view of the molecular gas distribution and motions within the central 9 kpc of M51 (Schinnerer et al. 2013). An analysis of the CO maps from this survey and the stellar population across the galaxy suggested that M51 has different zones of radially inflowing and outflowing gas. Regions of stalled gas are found at the transition between these zones, and there may be differences in the star-forming and cluster properties of the clouds in regions where gas moves differently (Meidt et al. 2013).

Previously, Sanchez-Gil et al. (2011) estimated the ages of the stellar populations in M51 from multi-wavelength (from far-UV through IR, and including Hα), low-resolution images, using a pixel-by-pixel approach. They found that the youngest ($<$4 Myr) stars are found along the central and inner edges of the inner spiral arms, and are spatially distinct from somewhat older 4–6 Myr stars, but did not track stellar populations older than 10 Myr. Scheepmaker et al. (2009) previously used *HST* images of M51 to detect individual star clusters and to estimate their ages, and found high concentrations of young ($\tau \lesssim$ 10 Myr) clusters along the spiral arms.

The goal of this work is twofold. First, we will define the spiral structures in both the inner and outer regions of M51 using the infrared emission from old stars to identify the stellar potential, and compare with the spiral structures traced by young stars, molecular gas, and dust. Second, we will compare the locations of age-dated star clusters from a new *HST*-based

catalog (Chandar et al. 2016) with different dynamical structures in M51, including spiral arms and "feathers" (stellar features extending from the outer portion of a spiral arm).

The remainder of this paper is organized as follows. Section 2 summarizes the selection and determination of star cluster properties presented in Chandar et al. (2016), and presents new maps showing the locations of clusters with different ages within M51. Section 3 defines the spiral arms from near-infrared images, which best trace the light from old stars, the dominant mass component in the inner disk. We also compare the locations of these stellar arms with those traced by very young clusters, molecular gas, and dust. In Section 4 we determine the spatial distributions of different age clusters relative to the spiral arms and feathers, and in Section 5 we compare our results with those predicted by different models of spiral structure generation. Finally, we summarize the main results of this work in Section 6.

2. Ages and Locations of Star Clusters in M51

The observations and basic reduction of the data used in this work were described previously in Chandar et al. (2011), and the cluster catalog is presented in Chandar et al. (2016), so here we summarize the relevant steps and refer the interested reader to those works for more details. M51 was observed in a 2 × 3 mosaic[9] with the Wide Field Channel of the Advanced Camera for Surveys (*ACS/WFC*) in the F435W ("*B*"), F555W ("*V*"), F814W ("*I*"), and the F658N ("Hα") filters as part of program GO-10452 (PI: S. Beckwith). The pixel scale of these observations is 0″05 pix^{-1}, or 2 pc pix^{-1} at the assumed distance of 8.4 Mpc for M51 (distance modulus $m - M = 29.62$; Feldmeier et al. 1997; Vinko et al. 2012). We also obtained six pointings with the F336W ("*U*") filter of the WFPC2 camera as part of program GO-10501 (PI: R. Chandar). Two additional archival F336W pointings cover the nuclear region of M51 (GO-5652, PI: R. Kirshner and GO-7375, PI: N. Scoville). Our *U*-band mosaic was shown in Figure 2 of Chandar et al. (2011), and has a resolution of 0″1 pix^{-1} corresponding to 4 pc pix^{-1}. It covers ≈60% of the luminous portion of the *ACS* mosaic.

We selected star clusters to be brighter than $V = 23.5$ (i.e., $M_V \lesssim -6$), and to be broader than the point-spread function. A final visual inspection to eliminate remaining close pairs of individual stars led to a catalog of 3812 cluster candidates, which was presented in Chandar et al. (2016). Circular aperture photometry was performed on each cluster in each broadband filter with an aperture radius of 2.5 pixels and background annuli of 10 and 13 pixels. We perform photometry for the narrowband Hα filter from an image where no flux from the stellar continuum was subtracted. The instrumental magnitudes were converted to the VEGAMAG photometric system by applying the zero-points given in Sirianni et al. (2005) for the ACS filters, and those given in Holtzmann et al. (1995) for the WFPC2 filter. Finally, we applied an aperture correction to the magnitudes measured for each source, based on an empirically determined relationship between concentration index (*C*) and aperture correction determined for a number of relatively isolated clusters.

Our cluster selection limit is several magnitudes brighter than the detection limit. We can detect nearly all objects

(except sometimes due to crowding) down to $V = 26$. However, our ability to cleanly separate clusters from point sources, close pairs of stars, and background galaxies worsens significantly at magnitudes fainter than $V \approx 23.5$. We assessed the completeness of our sample by adding artificial clusters throughout the image, and then subjecting them to our selection criteria. These experiments indicate that our sample is fairly complete (at ≈90% level) in most of M51. A similar level of completeness occurs closer to $m_V \approx 23.0$ mag in the most crowded portions of the spiral arms. We have confirmed, however, that the completeness limit does not affect the results presented here: the distributions presented in Section 6 are similar regardless of whether or not we use a limit of $m_V = 23.0$ or 23.5, but the shallower catalog yields poorer statistics.

Age and mass are two basic properties of a star cluster. Our methodology was described in detail in Chandar et al. (2016), and is summarized here. We estimate the age τ and extinction A_V for each cluster by performing a least χ^2 fit comparing observed magnitudes with the predictions from Bruzual & Charlot (2003) stellar population models assuming solar metallicity $Z = 0.02$, a Salpeter (1955) IMF, and a Galactic-type extinction law (Fitzpatrick 1999). The best-fit values of τ and A_V are those that minimize the statistic

$$\chi^2\left(\tau, A_V\right) = \sum_\lambda W_\lambda \left(m_\lambda^{\mathrm{obs}} - m_\lambda^{\mathrm{mod}}\right)^2, \qquad (1)$$

where m_λ^{obs} and m_λ^{mod} are the observed and model magnitudes, respectively, and the sum runs over all five bands, $\lambda = U, B, V, I$, and $F658N$. The weight factors in the formula for χ^2 are taken to be $W_\lambda = [\sigma_\lambda^2 + (0.05)^2]^{-1}$, where σ_λ is the formal photometric uncertainty determined by PHOT for each band. The mass of each cluster is estimated from the observed V-band luminosity, corrected for extinction, and the (present-day) age-dependent mass-to-light ratios (M/L_V) predicted by the models, assuming a distance modulus $\Delta(m - M)$ of 29.62 or 8.4 Mpc for M51 (Feldmeier et al. 1997; Vinko et al. 2012).

We test the sensitivity of our age-dating methodology to different stellar population models, and different assumptions (e.g., extinction law, metallicity, filter combinations). We find that cluster ages are fairly insensitive to the specific models that are used, as well as to the assumed metallicity (solar versus $1/2\times$ solar) and extinction law (Galactic versus Starburst). The most significant impact on the results comes from the specific filter combination. We tested the results from UBVIHα, BVIHα, and UBVI, and found that ≈35% of the clusters have ages that differ by at least 0.3 in log τ, with the UBVIHα combination delivering better ages (see the discussion in Section 3.2 in Chandar et al. 2016).

Figure 1 shows the spatial distribution of clusters with different ages on an optical image of M51. Figure 2 shows the same information, but now plots clusters in different intervals of age in separate panels on a white background. This figure shows that while structure in the cluster population clearly diffuses over time, clusters still retain some concentration in spiral patterns for a few hundred Myr; we will return to this point in Section 5.

---

[9] The observations and resulting mosaic images can be obtained at the following URL: http://archive.stsci.edu/prepds/m51/.
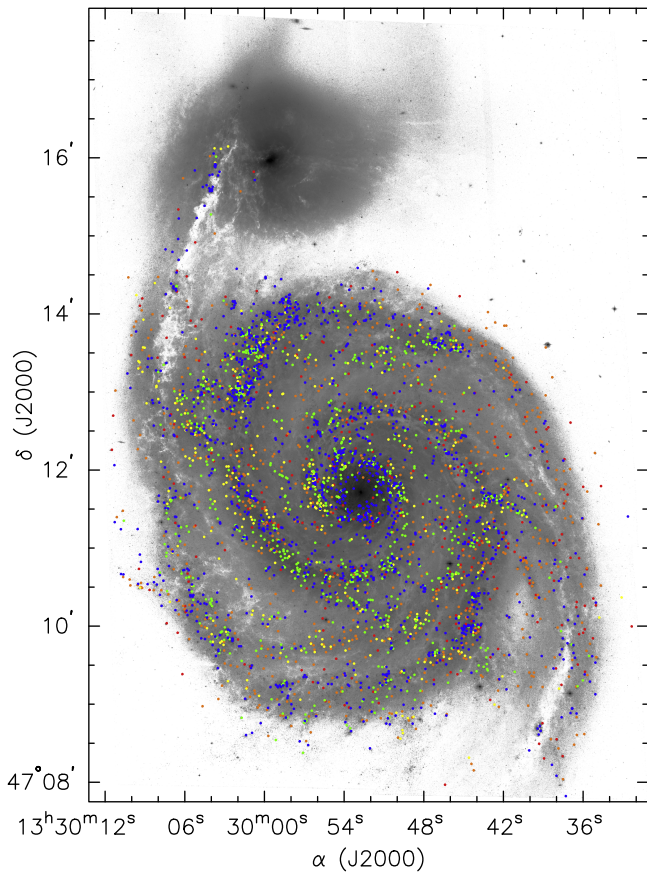
Figure 1. Distribution of clusters with different ages on the *HST* ACS image of M51: <6 Myr (blue); 6–30 Myr (green); 30–100 Myr (yellow); 100–400 Myr (orange); and >400 Myr (red). The lack of clusters in the very central portion of the galaxy is real.

3. Structural Features in M51

M51 has two prominent arms that wind clockwise with increasing distance from the center of the galaxy. In this section, we define the spiral arms in M51 from 3.6 μm images taken with the *Spitzer Space Telescope*, which reveal the old stellar backbone along the galaxy. We then compare these arms with the spiral structure observed in optical images (which highlight the locations of young stars and dust) and with that found in CO maps from the PAWS survey (which shows the locations of cold molecular gas). We also define four different feathers.

3.1. Spiral Arm Definitions

In Figure 3, we present a 3.6 μm image of M51 taken as part of the Spitzer Infrared Nearby Galaxies Survey (SINGS) Legacy project (Kennicutt et al. 2003). This image has a large field of view and covers both the inner and outer spiral arms. The emission in this image comes primarily from old stars, revealing the minimum in the stellar mass density potential. This image has a pixel scale of 0″.75 pix^{-1}.

We use the 3.6 μm image to define spiral arms in M51. First, we mask out the companion galaxy, the inner 750 pc region of M51, and bright point sources that appear to be unrelated to the arms, including bright foreground stars. This masked image is then subtracted from a median-averaged image and smoothed by a Gaussian with a FWHM of 12 pixels ($\simeq$0.6 kpc), a procedure that enhances the spiral arms. Finally, we identify 50

peaks along the spiral arms by running the DAOFIND task in IRAF. Both panels of Figure 3 show the resulting contours of the spiral arms and the identified peaks in orange.

We define different spiral arm segments, partly motivated by a previous analysis of CO maps that revealed that there are different dynamical zones within M51 (Querejeta et al. 2016). These zones are shown as the solid and dashed black circles in the left panel of Figure 3 (and also in Figure 5), and delineate regions where gas is moving radially inward from those where it is moving outward (the direction of gas motion in these zones is shown by the black arrows). The inner solid circle at 22″ ($\approx$830 pc) marks the corotation radius of the bar, and gas in this region flows inward. The inner dashed circle is located at 40″ ($\approx$1.5 kpc), and gas between 22″–40″ flows outward. The next dynamical zone, between 40″–100″ has inflowing gas, and the outer edge ($\approx$100″) of this zone marks the corotation radius of the spiral pattern in M51. The final zone, between 100″–165″ has outflowing gas, and the outer edge near $\approx$165″ is marked by the outer Lindblad resonance of the spiral. Our spiral arm segments, defined by fitting the 3.6 μm peaks with logarithmic spirals, are labeled and shown as the solid, colored lines: E1 (red), E2 (magenta), E3 (green), E4 (yellow) for the east arm extending toward the northeast, and W1 (dark blue), W2, (cyan), W3 (blue), W4 (purple), and W5 (dark pink), for the west arm extending toward the southwest.

Our spiral arm definitions are fairly similar to those presented in Scheepmaker et al. (2009), but the deeper 3.6 μm *Spitzer* image used here resulted in the detection of twice as many peaks and therefore somewhat smoother arm definitions. Honig & Reid (2015) recently used H II regions to define spiral arms in several galaxies including M51. Overall, the locations of their H II regions are quite similar to the very young (blue) clusters used in this work, which generally fall on the leading edge of the arms defined here.

3.2. Comparison with Optical Emission

We overlay the 3.6 μm contours showing our spiral arm definitions on top of an optical *HST* image of M51 in the right panel of Figure 3, and show an enlarged view of a portion of the inner eastern spiral arm in Figure 4. The infrared emission peaks, shown as the solid orange circles, wander somewhat relative to the dark dust lane and the brightest knots of optical emission from the recently formed young stellar clusters that punctuate the leading edge of the arms. Overall, this bright 3.6 μm emission (which is the basis of our spiral arm definitions) falls mostly somewhere between the two in the inner arms and in the outer east arm. The situation is somewhat different in the outermost portion of the west arm, where the brightest infrared emission appears to be coincident with the dust in the optical image. We will see throughout the rest of this paper that the outermost western spiral has different properties than the other spiral segments.

We estimate the typical offset, between the bright 3.6 μm emission that we have used to define the spiral arms and the dark dust lanes seen in the optical image using a few inner segments of the spiral arms (including the one that is shown). In the inner arms where the spiral pattern is the most regular, we find typical offsets in the range $\approx$0″.5–2″ or 20–80 pc. This will become important later when we compare the locations of age-dated clusters to the spiral arms defined by the 3.6 μm emission.
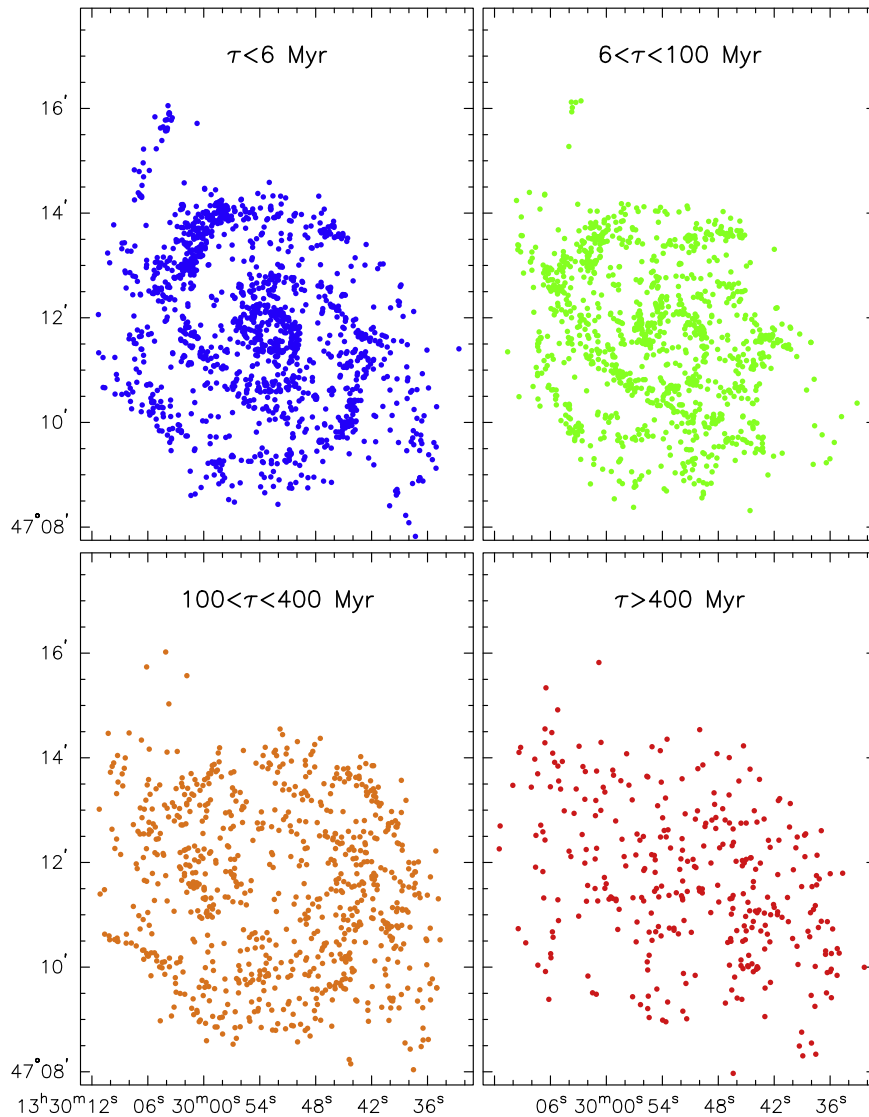
Figure 2. Gradual diffusion of clusters throughout the disk of M51. The clusters start out quite concentrated in the arms, and they become more and more dispersed as they age. Clusters with ages of a few hundred Myr do, however, still show weakly concentrated structure and are not yet fully dispersed. The color-coding is the same as in Figure 1: (<6 Myr (blue) 6–100 Myr (green); 100–400 Myr (orange); and >400 Myr (red).

3.3. Comparison with CO Emission

Figure 5 brings together the 3.6 μm image and spiral arm definitions, locations of optically detected star clusters, and maps of molecular gas that have been previously published. Here, the orange contours show ^{12}CO(1−0) molecular gas for the central 11×7 kpc of M51 from the PAWS survey (Schinnerer et al. 2013), covering the inner region. Cold molecular gas is concentrated in narrow spiral patterns starting $\approx$750 pc from the center. There are a number of "spurs" or small-scale physical extensions of gas from the arm into the interarm regions. Molecular gas is also found between the spiral arms, although the intensity of its emission is significantly lower than that in the arms. While CO emission was detected within the central $\sim$1 kpc of M51, it is fairly weak. The number of star clusters drops off significantly within the central $\approx$750 pc.

A visual comparison between the CO contours and an optical image shows that emission from the molecular gas coincides almost perfectly with the dark dust lanes found in the optical image of M51, while the bright emission from massive stars within stellar clusters is on the outer edge of the CO gas/dust lane. This offset is seen in Figure 5, with young star clusters ($\tau < 6$ Myr) shown as the blue dots offset toward the outer edge of the spiral pattern from the CO gas. We find a typical separation between the dark dust lanes and bright clusters of $\approx$5″–6″ or $\approx$200–240 pc for the inner spiral arm.

3.4. Comparison between Spiral Patterns in the Young and Old Stars, Gas, and Dust

The background image of Figure 5 is the 3.6 μm image that has been corrected for dust emission (Querejeta et al. 2015).[10] An enlarged version of this image, focusing on the inner spiral arms, is shown in Figure 6. Weak infrared emission is observed along the outer edge of the dust lanes/molecular gas; this infrared emission is the light of the old stars. We compare the locations of the dust lanes and the infrared emission in the inner

---

[10] We did not use this dust-corrected image to define the spiral arms because there are clear over-subtractions in some locations, which affected the locations of the detected infrared peaks. This map is better, however, for a visual comparison with emission at other wavelengths.
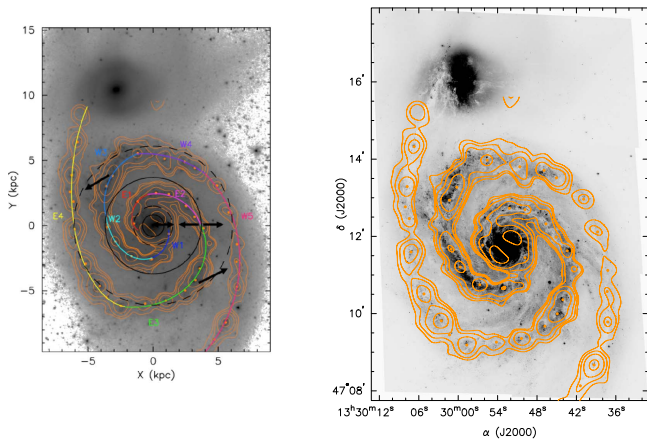
Figure 3. Left: definitions of M51 spiral arm segments are shown on a grayscale 3.6 μm *Spitzer* image. The orange contours show seven levels of intensity from 0.01 to 0.45 MJy/sr on a logarithmic scale, and the filled dots mark local intensity peaks. The fitted logarithmic arm segments are labeled and defined as E1 (red), E2 (dark pink), E3 (green), and E4 (yellow) for the east arm, and W1 (blue), W2 (cyan), W3 (light blue), W4 (purple), and W5 (magenta) for the west arm. The black circles define the different dynamical zones discussed in Section 3.1. Right: contours from the *Spitzer* 3.6 μm image (orange) are shown superposed on the optical *HST*/ACS image. In both the inner arms and the outer east arm, the strong infrared emission (orange circles) falls just beyond the dark dust lanes (which coincide with the molecular gas) in the direction of rotation. The orange circles also generally tend to be offset from the strongest optical emission, falling between it and the dust lanes in the inner portion of the spiral arms. The approximate offsets between the dust lanes, peak 3.6 μm emission, and optical emission are quantified in the text.
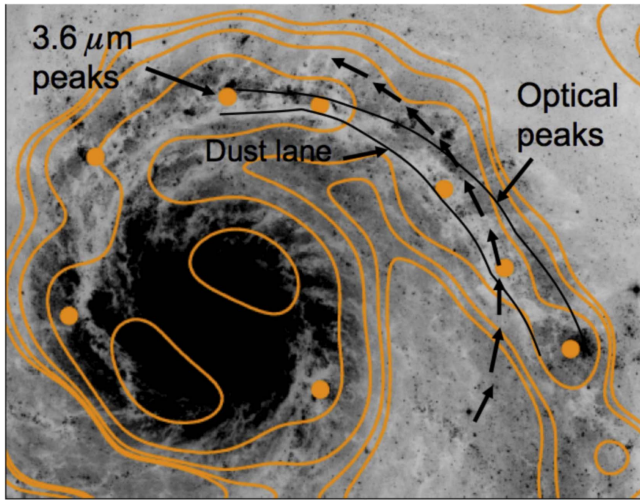
Figure 4. An optical image of a portion of the inner West spiral arm is superposed with the same infrared contours from *Spitzer* as seen in Figure 3 and shown in orange. The orange circles show the locations of the strongest 3.6 μm emission. Approximate locations for the dust lane (which is coincident with molecular gas) and the optical emission peaks are shown by the solid black lines and labeled. There is a progression from the optical peaks, to the 3.6 μm peaks, to the location of the dust from the outer edge of the spiral arm inward. Typical values for these offsets are given in the text. The arrows show the sense in which gas and stars moving in elliptical orbits rotate in the M51 disk, and how they travel along the arm for part of their orbits, which appears to result in clusters lingering in spiral arms and traveling quickly between them.

arms and find a typical offset between $\approx 2''$–$5''$ or ≈ 80–200 pc. A comparison of an 8 μm image from *Spitzer* (see Figure 10 in Puerari et al. 2014) with the 3 μm image used here to define the stellar spiral arms reveals that the diffuse gas structure is offset from and less well-defined than the stars in W3 and E3.
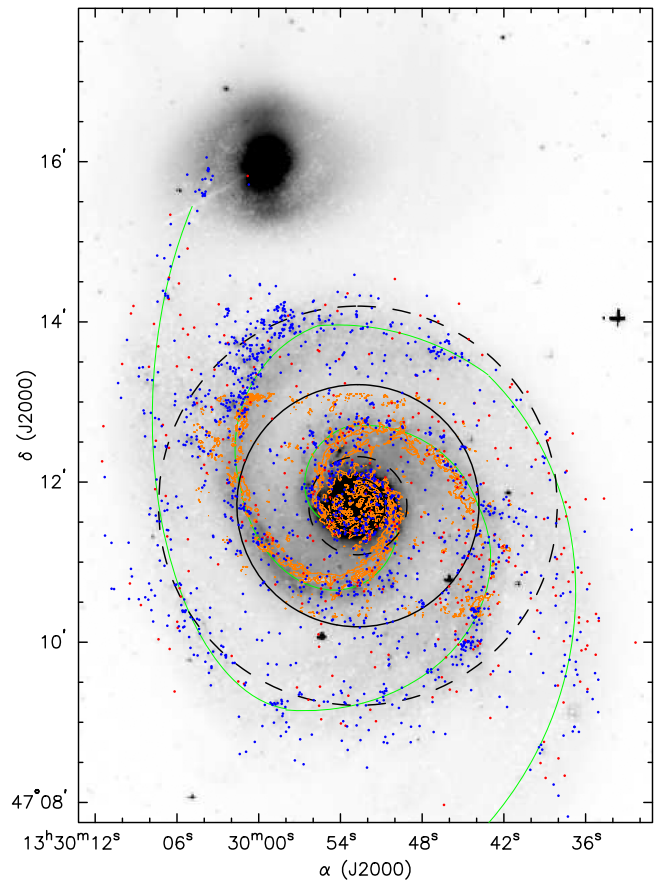

Figure 5. This figure compares the locations of optically bright star clusters (small dots, Section 2), both very young (blue dots; $\tau \lesssim 6$ Myr) and old (red dots; $\tau > 400$ Myr), with our definition of the spiral arms (curved lines; Section 3) and cold CO molecular gas (orange contours from the PAWS survey; Schinnerer et al. 2013). The background image is a 3.6 μm *Spitzer* image that shows the stellar mass distribution of the galaxy (Querejeta et al. 2015).

The various offsets suggest the following picture for the organization of spiral structure in M51: cold molecular gas (traced by both CO emission and dark dust lanes in the optical) defines the inner edge of the spiral structure in M51. Bright 3.6 μm emission from an overdensity of old stars (the definition of spiral arms adopted in this work) are on the outer edge of this gas, followed even further out by optically bright young stellar clusters.

In addition to the spiral arms, in this work we will discuss the location and ages of clusters in "feathers," coherent stellar structures emanating from the spiral arms. These should not be confused with the many extinction features located between the arms that were identified by La Vigne et al. (2006). We identify four such stellar structures in an optical image of M51 shown in Figure 7; these structures can also be seen in the stellar density map, and are not affected by oversubtraction. The feathers contain star clusters, have larger pitch angles than the spiral arms, and appear to be a continuation of dark extinction and CO features (which we refer to as "spurs"; La Vigne et al. 2006). Figure 7 identifies four feathers in M51.

4. Spatial Distributions of Different Age Clusters

Figures 1 and 2 show the spatial distributions of clusters with different ages in M51. The youngest clusters, those with ages less than 6 Myr (shown in blue), are preferentially located close
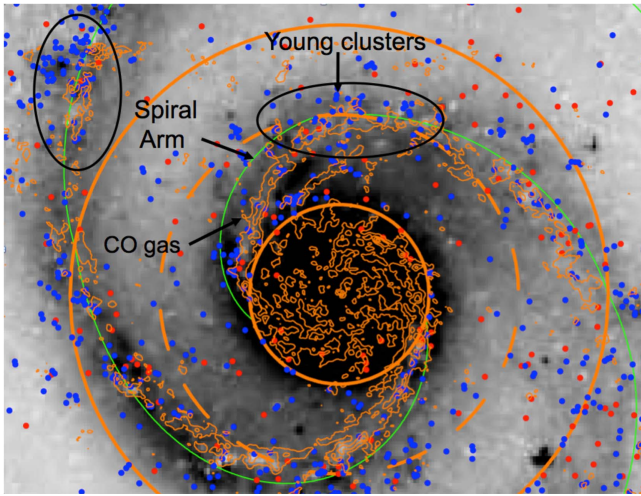
Figure 6. Portion of the inner spiral arms shown in Figure 5. The stellar density map created from a processed 3.6 μm image is overplotted with CO contours in orange, which coincide with the dust lanes. Our spiral arm definitions are shown in green, and tend to be just outside of the CO emission/dust, although the exact distance varies somewhat. The blue dots show that very young ($\tau \lesssim 6$ Myr) star clusters tend to be located beyond our definition of the inner spiral arms, and coincide fairly well with the infrared emission in this image. The locations of the infrared emission here are fairly similar to those of the optical emission in Figure 4. We highlight two portions of the spiral arm where the progression from CO gas/dust to spiral arm to young clusters is clearly observed.
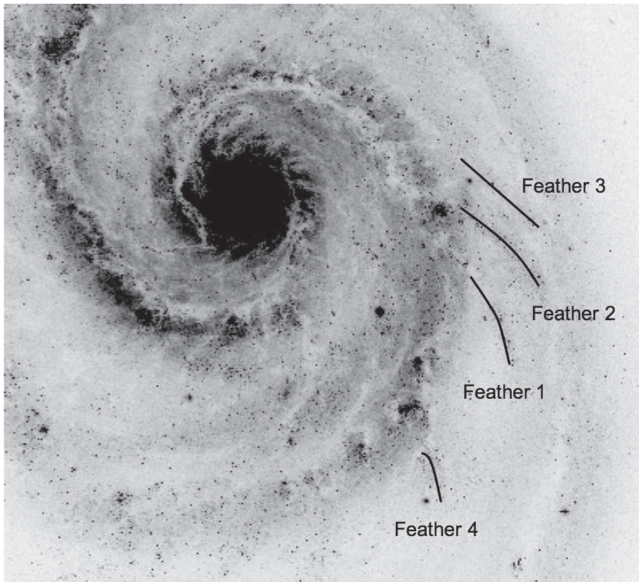
Figure 7. Locations of "feathers" discussed in this work.

to (but not coincident with) the densest portion of the spiral arms, as defined in Section 3. These very young clusters also tend to clump together, which can be seen in Figure 2. Note, however, that some very young clusters are also occasionally found between the spiral arms. This is not due to inaccuracy in our age-dating method. Hα emission, seen in the Hubble Heritage image of M51[11] is also observed at these locations, indicating that at least some recent star formation does occur between the arms (discussed further below).

---

[11] hubblesite.org/gallery/album/heritage/pr20050212a/small_web

Somewhat older clusters with ages between 6 and 30 Myr (green) and 30–100 Myr (yellow) are still found close to spiral arms, although they clearly have a larger spread away from the arms than the very youngest clusters. Even intermediate-age clusters, those that are ≈100–400 Myr old and shown in orange, retain some knowledge of the initial spiral structure, and have not fully diffused throughout the disk of M51. This is discussed further below. The oldest clusters ($\gtrsim 400$ Myr; red), meanwhile, show a fairly even distribution throughout the galaxy, including across the spiral arms. The exception to these trends is arm segment W5, which is dominated by approximately 100–400 Myr old clusters, with almost no young clusters close to or within the arm. The latter observation is supported by a visual inspection of Figure 1, which shows far fewer H II regions in W5 than in any other arm segment. This feature will be discussed further below. Young clusters continue to form in the outer arm E4, and are fairly tightly concentrated to the arm.

4.1. Cluster Ages Relative to Spiral Structure

In this section, we present a quantitative treatment of the locations of star clusters of different ages in M51, relative to the spiral arms, as defined by the old stellar backbone revealed in the 3.6 μm images. A cluster is associated with an arm segment when it is within 2 kpc of that segment, where distance is calculated from the cluster position to the closest point in the arm segment. Clusters near the intersection points of two arm segments could potentially be associated with either segment. In these cases, we define horizontal or vertical boundaries and manually assign the clusters to an arm segment.

Figure 8 shows the distribution of different age clusters perpendicular to the spiral arm segments E1, E2, E3, and E4. Each age distribution is normalized to the total number of clusters in its arm segment: 231 (E1), 287 (E2), 654 (E3), and 454 (E4), respectively. Each row shows the distribution of clusters with different ages: younger than 6 Myr (top row), 6–30 Myr (second row), 30–100 Myr (third row), and 100–400 Myr (bottom row). Figure 9 shows a similar plot for clusters in the west arm segments, with 205 (W1), 352 (W2), 581 (W3), 206 (W4), and 190 (W5) clusters, respectively. Note that the abrupt cutoff below −1 kpc for E1 and W1 is due to our exclusion of the central 750 pc region of M51.

We see from Figures 8 and 9 that there is a general trend for the youngest cluster distributions to be fairly peaked close to the spiral arm segments (although the distributions are not fully symmetric), and that the distributions become flatter and broader for older clusters, but that even clusters in our 100–400 Myr interval are still found in the arms. The one exception to this trend is the 100–400 Myr clusters in the W5 (and to a lesser extent W4) segment, which peak quite strongly at the arm. The overdensity of intermediate-age 100–400 Myr old clusters near the spiral arms is likely due to the fact that clusters spend much more time moving through the arms than through the interarm regions; see the discussion of simulation results in Section 5.

Two of the main results of this work can be seen even more clearly in Figure 10, where we compare the azimuthal distribution of molecular gas with young ($\tau < 10$ Myr) and intermediate-age (100–400 Myr) clusters in portions of the inner and outer spiral. Figure 10(a) shows the annuli that are used for the azimuthal plots: 2.0–2.5 kpc for the inner spiral and 5.0–5.5 kpc for the outer one. The azimuthal angles start
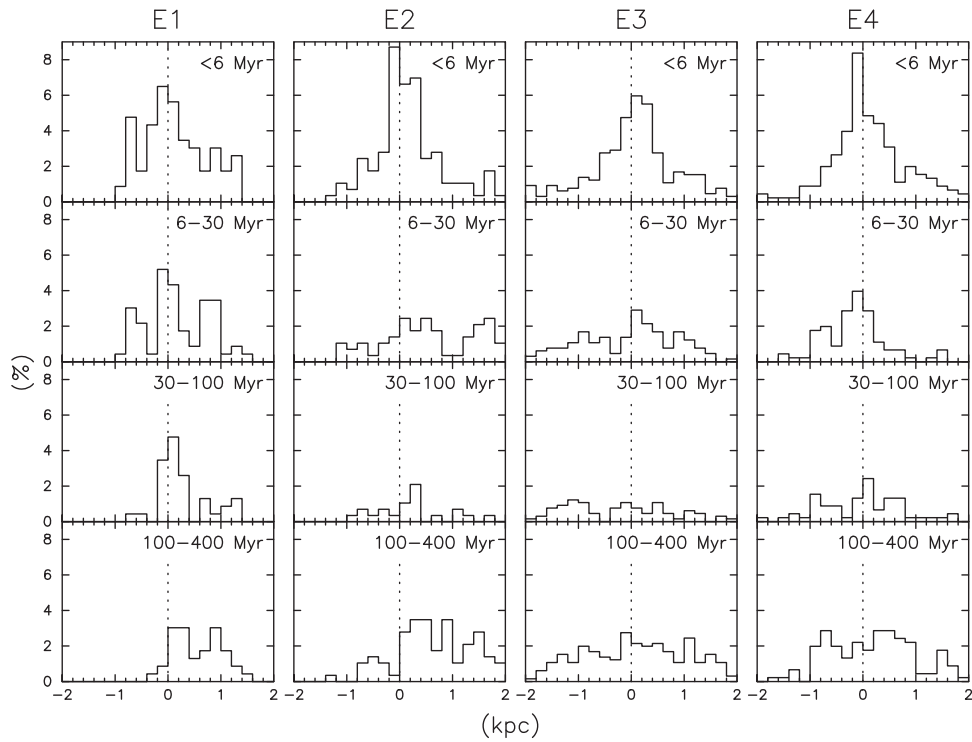
Figure 8. Spatial distribution of clusters perpendicular to the arm segments in each age group for the east arm. Each distribution is normalized to the total number of clusters in its arm segment. Distances (in kiloparsecs) of clusters are relative to the center of the arm (0 kpc) as defined in the 3.6 μm image, where positive distances represent clusters on the outer side of the arm, and negative distances represent clusters on the inner side of the arm.
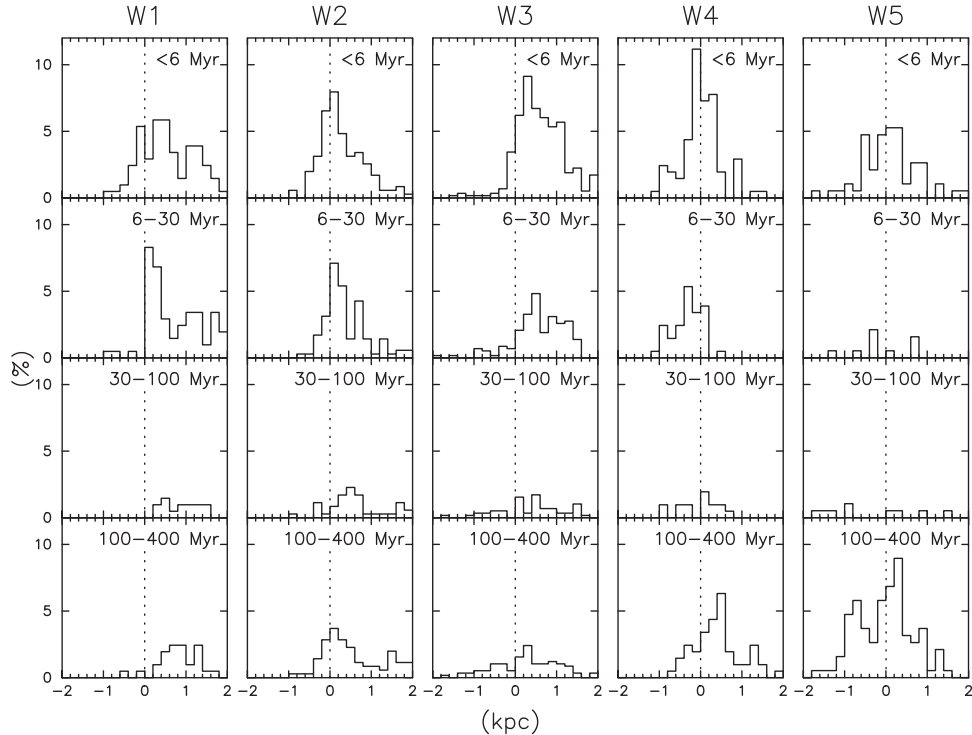
Figure 9. Same as Figure 8 but for regions in the west arm.

from north and go counterclockwise. Because the PAWS survey did not map the molecular gas content in the outer portion of M51, we use data from the lower spatial resolution HERACLES survey (Leroy et al. 2009) for the outer spiral arm. Figure 10(b) shows that HERACLES data give a fairly similar azimuthal profile as PAWS for the inner spiral for our bin sizes,

suggesting that the HERACLES maps are adequate for our purposes. Here, the y-axis is expressed in terms of H_2 surface density $(M_\odot \, pc^{-2})$, where we have assumed a (Galactic) conversion factor of $\alpha_{CO} = 4.4 \, M_\odot \, pc^{-2} \, K^{-1} \, km^{-1} \, s$ (Schinnerer et al. 2013). The lower panels compare the azimuthal profiles of molecular gas with that of young $(\tau \lesssim 10 \, Myr)$ and intermediate-
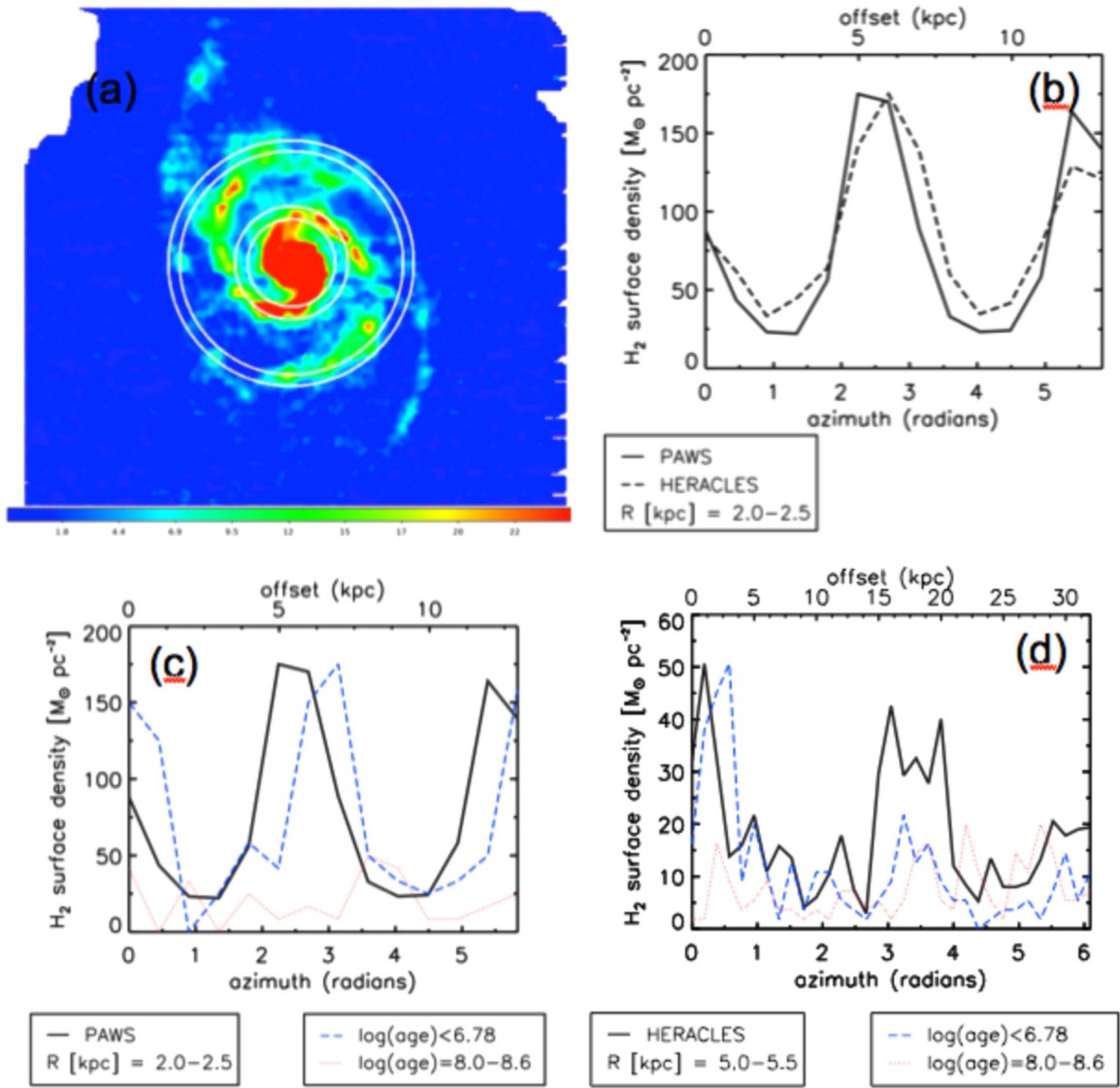
Figure 10. Azimuthal distribution of CO gas and very young $\tau \lesssim 6$ Myr and intermediate-age 100–400 Myr clusters. The cluster distributions have been plotted in 1 kpc wide bins. The distribution of young clusters (dashed blue lines) has been normalized to match the peak of the azimuthal gas surface density (it is expressed in arbitrary units), but the intermediate-age cluster distribution is normalized relative to the young cluster population so that the different amplitudes in the young and intermediate-age clusters reflect the differences in their numbers. The peak in the cluster populations is clearly offset, by ≈ 1 kpc, from that of the molecular gas. The distribution of older clusters is broader than that for younger ones, but still shows a weak concentration at the same location as very young clusters.

age (100–400 Myr) clusters in the inner (bottom left) and outer (bottom right) annuli. The molecular gas, plotted as the solid line, shows strong peaks at both spiral arms. For the inner spiral, the blue dashed line shows fairly narrow peaks for the young clusters, and shows that these peaks are offset by ≈ 1 kpc from the peaks in the molecular gas. There are far fewer older clusters, reflected by the lower amplitude of the red line, and they appear to be more evenly distributed than the young clusters. These spatial offsets between the peaks in the gas and cluster profiles support the density wave model for the inner spiral of M51. The situation, however, changes in the outer spiral. Here, the broad peak observed between 2.5 and 4 radians in CO gas appears to be fairly cospatial with the (few) young and intermediate-age clusters in this region, suggesting that a different mechanism is responsible for the outer spiral structure.

From Figures 11 and 12, we see that the different arm segments have had different amounts of recent star formation,

with strong recent cluster formation in segment W3, and to a lesser extent in E3. Gas is flowing in these segments, which might be expected to suppress rather than to enhance star formation (e.g., Meidt et al. 2013). The movement of gas in these segments, which are outside of the spiral corotation radius, may be dominated by flows resulting from the interaction with the companion galaxy, rather than flows along or through the underlying spiral. In W3, the dominant young cluster concentration is offset by ≈ 0.5 kpc toward the companion galaxy; this offset is likely due to the ongoing interaction with the companion galaxy.

As mentioned previously, arm segment W5 appears to be quite different from the other segments. This segment contains very few young clusters (there are very few regions of Hα emission), and is dominated by clusters with ages of 100–400 Myr. This result is consistent with this outer region being part of a material arm; simulations show that material
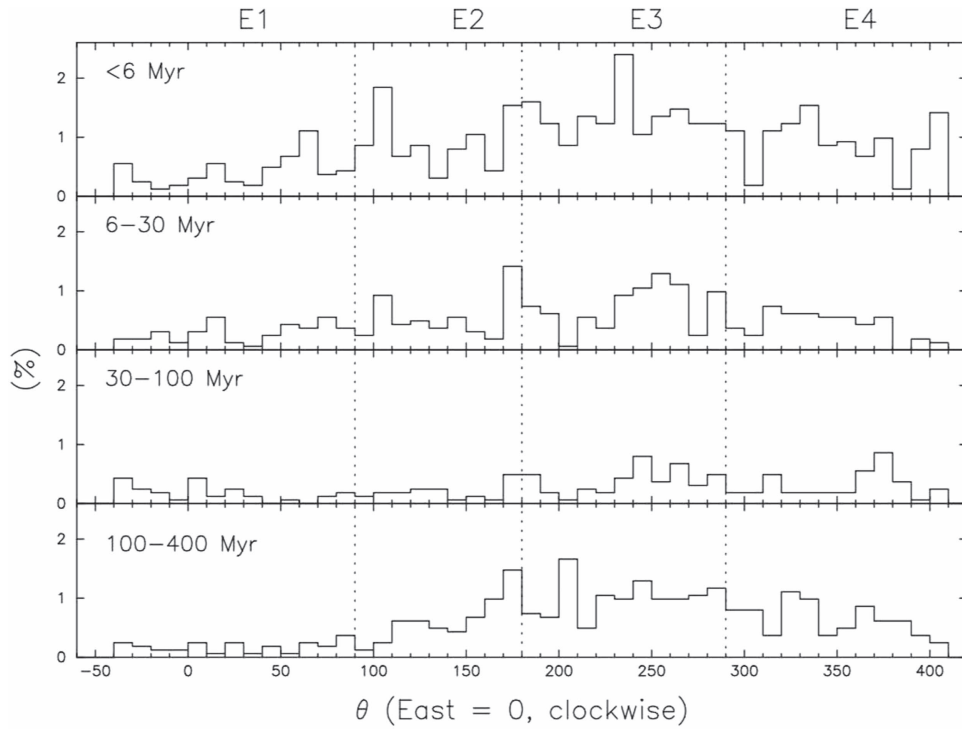
Figure 11. Distribution of clusters along the east arm in each age group. Here, each distribution is normalized to the total number in the east arm ($N = 1626$). $\theta = 0$ is defined as the point that is directly east of the galaxy center (in segment E1), and θ increases clockwise toward the outer arm. The dotted lines show the edges of each arm segment defined in Figure 3.
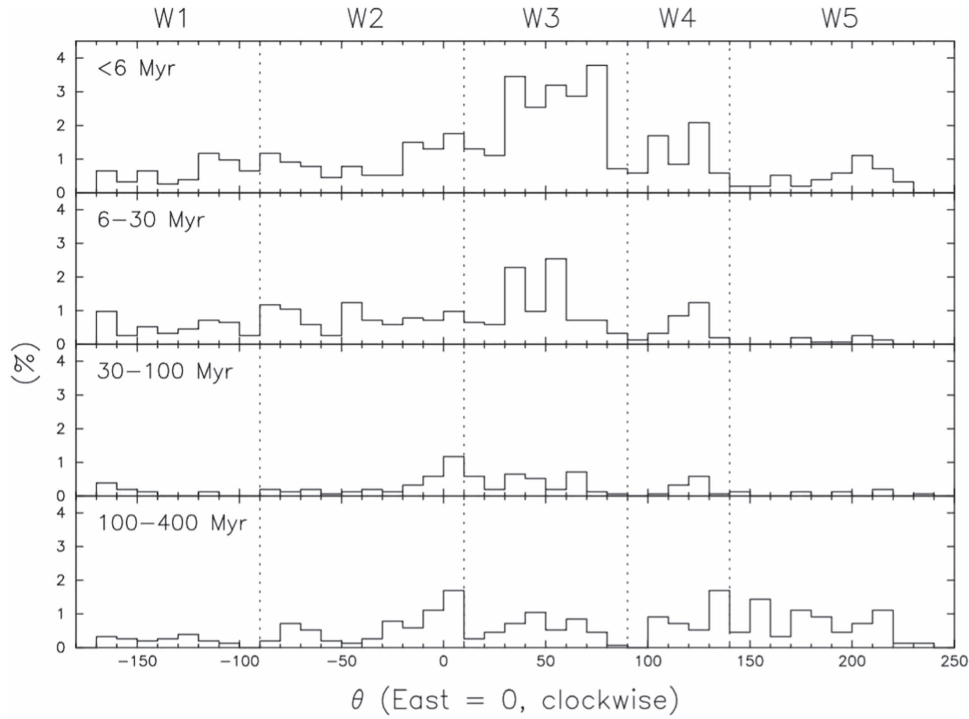

Figure 12. Same as Figure 11 but for the west arm. Here, each distribution is normalized to the total number of clusters in the west arm ($N = 1534$), and $\theta = 0$ is the point directly east of the galaxy center in segment W2.

arms can hold onto their star clusters for many rotations (Dobbs & Pringle 2010). The lack of recent star formation is also consistent with the fairly low amount of gas in W5 when compared with the higher gas content and star formation rate in outer arm E4.

4.2. Ages of Clusters In Feathers

M51 has several coherent stellar "feathers" emanating from the spiral arms, identified in Figure 7. These contain star clusters, have larger pitch angles than the spiral arm, and appear to be a continuation of dark extinction features (we refer
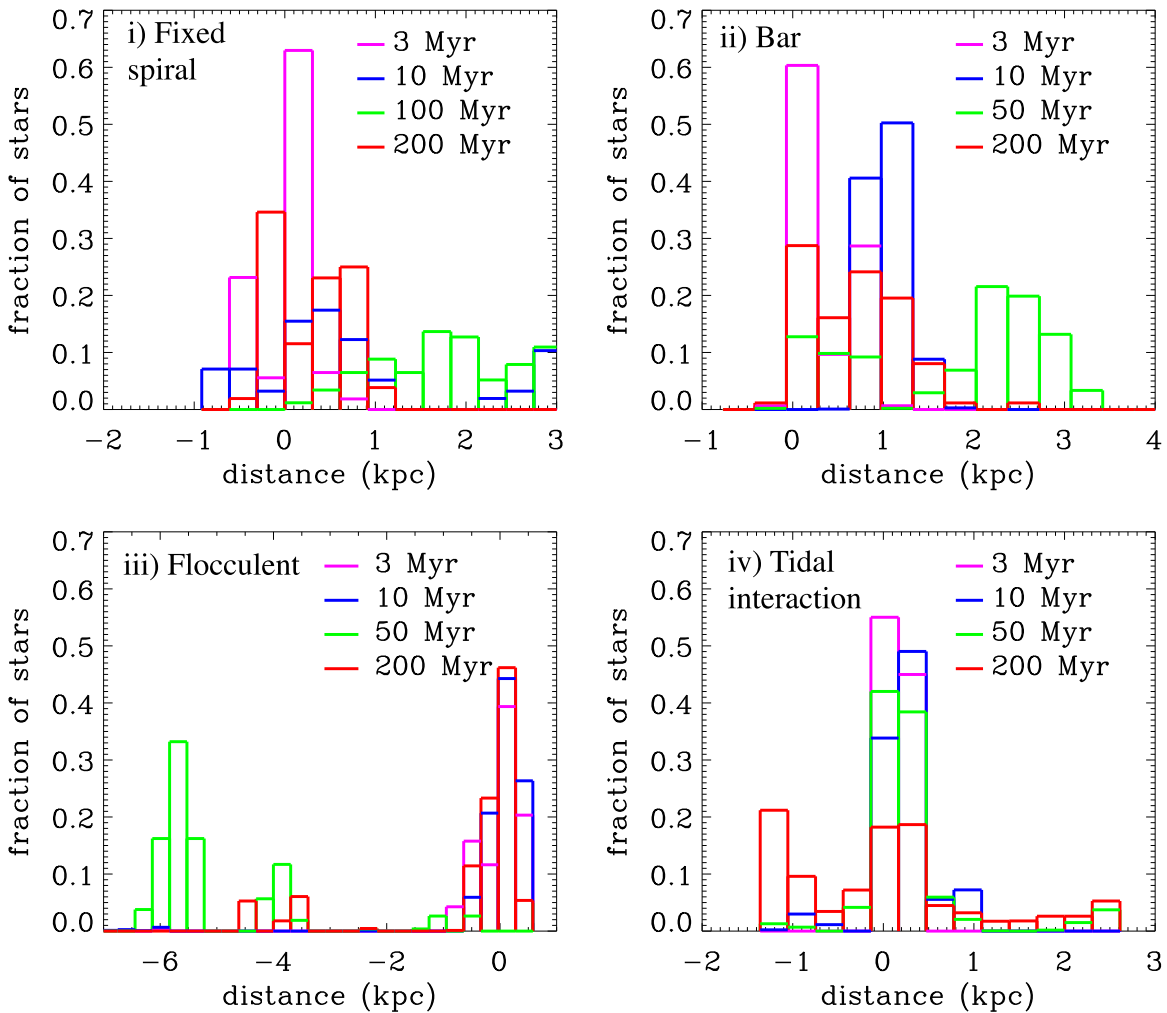
Figure 13. Histograms showing the distribution of clusters across spiral arms for the four spiral generation models shown in Figure 2 of Dobbs & Pringle (2010): spiral with a fixed pattern speed (top left), a barred galaxy (top right), a flocculent spiral (bottom left), and a tidally induced spiral based on the M51 system (bottom right). Four different age clusters are shown for each simulation, as indicated. The center of the spiral arm is assumed to coincide with the location of the peak of the youngest cluster distribution, and positive positions are downstream from the spiral arm.

to these extinction features as "spurs"). We studied the ages of clusters in two of the most prominent stellar feathers in a previous paper (Chandar et al. 2011), and here extend our analysis to include two additional structures.

We previously found that the clusters in feather 1, one of the most coherent stellar structures, formed nearly coevally, ≈100 Myr ago. We also noted that one of the most massive clusters in M51 is located within feather 1. Clusters in feather 2 appear to be somewhat older on average, with a typical age of $\tau \approx 200$ Myr, but also appear to have formed over a longer period of time. Here, we identify and examine the cluster content of feathers 3 and 4 for the first time. These features are less coherent than feathers 1 and 2, and can be traced over shorter distances. Overall, feather 3 appears to have similar ranges and median cluster ages as feather 2, which is just to the south. Feather 4, however, has a larger age spread than any of the other three feathers, and is also the least coherent. Most importantly, we do not see evidence for age gradients along any of the feathers, as might be expected if star formation had been triggered at one end and propagated across to the other end. Rather, these features are consistent with clusters forming out of gas that has been sheared out as it moves through the arms.

5. Comparison with Simulations

A number of works have used hydrodynamical simulations to study the response of the gas disk to different mechanisms for generating spiral structure. These simulations track the expected locations of different age stars and clusters and make predictions that can be compared with observations. For a fixed density wave, there should be spatial offsets for different age tracers; such as, for example, between molecular gas and young clusters, as material streams in and out of the spiral pattern (e.g., Roberts 1969 Dobbs & Pringle 2010). In the global spiral density wave simulation of Dobbs & Pringle (2010), the youngest clusters are all tightly confined to the spiral arms, with older ~100 Myr clusters found at similar locations but more spread out than the younger clusters, as shown in the top left panel of Figure 13. In a flocculent galaxy, where the spiral structure results from local gravitational instabilities in the disk, no offsets between gas and young clusters are necessarily expected, and clusters with different ages are not cospatial (see the bottom left panel in Figure 13; Dobbs & Bonnell 2008; Wada et al. 2011). In some models of spiral arm generation, gas and star clusters spend much more time *in* the spiral arms than *between* the arms, since they stream parallel to the arm, in a fashion similar to that shown by the arrows in Figure 4. In these

simulations, clusters move slowly through the arms and quickly through the interarm regions, and if not dispersed by feedback, clusters with ages up to a few hundred Myr are predicted to respond to the potential and exhibit a spiral pattern (e.g., Dobbs et al. 2016).

We find some intriguing similarities and differences when we compare the observational results and different model predictions. In M51, different age clusters all peak at the spiral arms (as discussed in Section 4), but the widths of the distributions increase somewhat at older ages, similar to predictions from the fixed spiral model of Dobbs & Pringle (2010). Recent simulations find that spiral structure tends to persist for hundreds of Myr, but no corresponding structure was found in similar age cluster populations in NGC 628, M83, or NGC 1566 (Dobbs et al. 2016). Interestingly, in this work we do observe this signature in the few-hundred-Myr cluster population of M51.

The cluster population associated with the inner spiral arms of M51 is consistent with predictions from density wave simulations. Different age clusters peak at the spiral arms, and the widths of the distributions increase with age. Spatial offsets are observed between the molecular gas and young clusters. We note, however, that the width of the spatial distributions for very young clusters (and in many cases for older clusters as well) across spiral arms is significantly narrower in the simulations (as shown in Figure 13) than is observed in M51. In the simulations, clusters are assumed to form as soon as gas reaches some density threshold; based on our results, this assumption may be too simplistic, as also suggested by other recent work (e.g., Schinnerer et al. 2017).

In the flocculent model, by contrast, the peak locations vary strongly with age, but the height and width do not. Both the locations of the peaks and widths of different age cluster distributions vary in the model with a central bar. The flocculent and barred models are a poor match to the observed results for clusters in M51.

Feathers, or spurs, are also seen in numerical simulations, with a fixed spiral potential (Kim & Ostriker 2002; Wada & Koda 2004; Shetty & Ostriker 2006, Dobbs & Bonnell 2006), and more recently for an interacting galaxy (Pettitt et al. 2016). Feathers are formed in the simulations when GMCs in the spiral arms are sheared out in the interarm region. Dobbs et al. (2014) compute stellar age distributions in GMCs located in feathers (or effectively the feathers themselves) and arm GMCs. The clusters have a large age spread in the feathers, as the feathers correspond to long-lived GMCs, which form stars over a long lifetime. Shorter-lived GMCs, on the other hand, are already dispersed by the time they reach the interarm region. Equivalent analysis has not yet been performed for simulations of interacting galaxies. For flocculent galaxies, gas does not pass through the spiral arms, so feathers cannot form in the same way (Dobbs & Bonnell 2008; Wada et al. 2011). Instead, any such features would simply be short sections of spiral arm, so presumably their age distributions would reflect this.

Overall, the fixed spiral simulation is best able to reproduce (at least) some of the general trends observed in the cluster population in the inner portion of M51, while the flocculent and barred galaxy models do a much poorer job of reproducing the observations. The outer spiral seems to be best reproduced in the interaction model of Dobbs et al. (2010), and is more consistent with being a material arm rather than a density wave.

6. Summary

We have defined the spiral arms in M51 from a deep 3.6 μm image taken with the *Spitzer Space Telescope*, which traces the old stellar backbone of the galaxy, and compared this image with the spiral structure observed at optical and radio wavelengths. We found the following approximate sequence for the locations of stars (young and old), gas, and dust. Optical light at bluer wavelengths from *HST* images traces the youngest, brightest stars and clusters, which are found along the outer edge of the arm. The infrared 3.6 μm images revealed that the older stars mostly trail the young, optically bright clusters by about $2''$ in the inner arms. This stellar mass overdensity is followed by the dust lanes and molecular gas, which are concentrated into very narrow spiral structure (in the inner arms).

We have compared the locations of age-dated star clusters in M51, from the *HST*-based catalog of Chandar et al. (2016), with different dynamical structures within the galaxy, including the spiral arms and stellar feathers. Our spiral arms were divided into different segments that coincide with the locations of distinct dynamical zones found previously by Meidt et al. (2013). The stellar feathers were visually identified in optical *HST* images of M51. We determined the spatial distributions of clusters in the following ranges of age: (1) $\tau \lesssim 6$ Myr, (2) 6–30 Myr, (3) 30–100 Myr, (4) 100–400 Myr, and (5) $\tau \gtrsim 400$ Myr.

Our key findings were:

1. Few clusters are detected within ≈ 750 pc of the center of M51.
2. Clusters with a range of ages, up to a few hundred Myr, are located within the spiral arms. In fact, the spatial distributions for different age clusters all peak close to the spiral arms, although the peak height decreases and the width increases with cluster age. This result, plus the spatial offset found between the molecular gas and clusters, supports a density wave origin for the spiral structure in the inner arms of M51.
3. The outer arm segment W5 (closest to the companion) contains primarily intermediate-age clusters, with very few young clusters. This differs from the eight other arm segments studied here, and suggests that this is a material arm.
4. We identify four "feathers," stellar structures beyond the inner spiral arm with a larger pitch angle than the arms. None of these show evidence for an age gradient along the structure, and the least coherent feathers appear to have the largest range of cluster ages.

References

Bastian, N., Gieles, M., Goodwin, S. P., et al. 2008, MNRAS, 389, 223
Bruzual, G., & Charlot, S. 2003, MNRAS, 344, 1000
Chandar, R., Whitmore, B. C., Calzetti, D., et al. 2011, ApJ, 727, 88
Chandar, R., Whitmore, B. C., Dinino, D., et al. 2016, ApJ, submitted

Colombo, D., Hughes, A., Schinnerer, E., et al. 2014a, ApJ, 784, 3
Colombo, D., Meidt, S., Schinnerer, E., et al. 2014b, ApJ, 784, 4
Dobbs, C. L., & Bonnell, I. A. 2006, MNRAS, 367, 873
Dobbs, C., & Bonnell, I. 2008, MNRAS, 385, 1893
Dobbs, C., & Pringle, J. E. 2010, MNRAS, 409, 396
Dobbs, C., & Pringle, J. E. 2010, MNRAS, 409, 396D
Dobbs, C. L., Pringle, J. E., & Naylor, T. 2014, MNRAS, 437, 31
Dobbs, C. L., Price, D. J., Pettitt, A. R., Bate, M. R., & Tricco, T. S. 2016, MNRAS, 461, 4482
Egusa, F., Kohno, K., Sofue, Y., Nakanishi, H., & Komugi, S. 2009, ApJ, 697, 1870
Emsellem, E., Renaud, F., Bournaud, F., et al. 2015, MNRAS, 446, 2468
Feldmeier, J., Ciardullo, R., & Jacoby, G. H. 1997, ApJ, 479, 231
Fitzpatrick, E. L. 1999, PASP, 111, 63
Foyle, K., Rix, H.-W., Dobbs, C. L., Leroy, A. K., & Walter, F. 2011, ApJ, 735, 101
Holtzmann, J., Burrows, C. J., Casertano, S., et al. 1995, PASP, 107, 1065
Honig, Z. N., & Reid, M. 2015, ApJ, 800, 53
Hughes, A., Meidt, S., Schinnerer, E., et al. 2013, ApJ, 779, 44
Kennicutt, R. C., Armus, L., Bendo, G., et al. 2003, PASP, 115, 928
Kim, W-T, & Ostriker, E. C. 2002, ApJ, 570, 132

La Vigne, M. A., Vogel, S. N., & Ostriker, E. V. 2006, ApJ, 650, 818
Leroy, A. K., Walter, F., Bigiel, F., et al. 2009, AJ, 137, 4670
Meidt, S., Schinnerer, E., Garcia-Brillo, S., et al. 2013, ApJ, 779, 45
Pettitt, A. R., Tasker, E. J., & Wadsley, J. W. 2016, MNRAS, 458, 3990
Puerari, I., Elmegreen, B. G., & Block, D. L. 2014, AJ, 148, 133
Querejeta, M., Meidt, S., Schinnerer, E., et al. 2015, ApJS, 219, 5
Querejeta, M., Meidt, S., Schinnerer, E., et al. 2016, A&A, 588, 33
Renaud, F., Bournaud, F., Emsellem, E., et al. 2013, MNRAS, 436, 1836
Roberts, W. W. 1969, ApJ, 158, 123
Salpeter, E. 1955, ApJ, 121, 161
Sanchez-Gil, M. C., Jones, D. H., Perez, E., et al. 2011, MNRAS, 415, 753
Scheepmaker, R. A., Lamers, H. J. G. L. M., Anders, P., & Larsen, S. S. 2009, A&A, 494, 81
Schinnerer, E., Meidt, S. E., Colombo, D., et al. 2017, ApJ, 836, 62
Schinnerer, E., Meidt, S., Pety, J., et al. 2013, ApJ, 779, 42
Shetty, R., & Ostriker, E. C. 2006, ApJ, 647, 997
Sirianni, M., Jee, M. J., Bentez, N., et al. 2005, PASP, 117, 1049
Tamburro, D., Rix, H.-W., Walter, F., et al. 2008, AJ, 136, 2872
Vinko, J., Takats, K., Szalai, T., et al. 2012, A&A, 540, 93
Wada, K., Baba, J., & Saitoh, T. R. 2011, ApJ, 270, 363
Wada, K., & Koda, J. 2004, MNRAS, 349, 270